Femtosecond time-resolved photoelectron spectroscopy with a Vacuum-Ultraviolet photon source based on laser high-order harmonic generation

Philippe Wernet*, Jérôme Gaudin§, Kai Godehusen, Olaf Schwarzkopf, Wolfgang Eberhardt

Helmholtz-Zentrum Berlin für Materialien und Energie GmbH, Albert-Einstein-Strasse 15, 12489 Berlin, Germany

* contact E-mail: wernet@helmholtz-berlin.de

PACS numbers: 32.80.Fb, 33.60.+q, 82.53.Eb, 42.65.Ky

$ Permanent address: European XFEL, Albert-Einstein-Ring 19, 22761 Hamburg, Germany

Abstract

A laser-based tabletop approach to femtosecond time-resolved photoelectron spectroscopy with photons in the vacuum-ultraviolet (VUV) energy range is described. The femtosecond VUV pulses are produced by high-order harmonic generation (HHG) of an amplified femtosecond Ti:sapphire laser system. Two generations of the same set up and results from photoelectron spectroscopy in the gas phase are discussed. In both generations a toroidal grating monochromator was used to select one harmonic in the photon energy range of 20-30 eV. The first generation of the set up was used to perform photoelectron spectroscopy in the gas phase to determine the bandwidth of the source. We find that our HHG source has a bandwidth of 140±40 meV. The second and current generation is optimized for femtosecond pump-probe photoelectron spectroscopy with high flux and a small spot size at the sample of the femtosecond probe pulses. The VUV radiation is focused into the interaction region with a toroidal mirror to a spot smaller than 100 x 100 μm^2 and the flux amounts to 10^{10} photons/s at the sample at a repetition rate of 1 kHz. The duration of the monochromatized VUV pulses is determined to be 120 femtoseconds resulting in an overall pump-probe time resolution of 135±5 fs. We show how this set up can be used to map the transient valence electronic structure in molecular dissociation.

I. INTRODUCTION

The generation of high-order harmonics of a femtosecond (fs) Ti:sapphire laser is an established method for creating femto- and attosecond light pulses with photon energies from the VUV to the x-ray range (1-3 and references therein). Often, the technological and methodological challenges for the generation and application of attosecond pulses are very different from those for femtosecond pulses. As we are describing our approach with femtosecond resolution we shall concentrate in the following on femtosecond pulses from High Harmonic Generation (HHG) (1, 2, 4-15). The applications of such pulses range from spectroscopy (1, 2, 16-27) to microscopy (28, 29) and coherent diffraction or holography (30-33). In most cases, HHG is performed with a driving-laser wavelength of around 800 nm and HHG pulses with photon energies between 15 and 100 eV are used. It has been shown in recent studies that the photon energy range can be considerably extended into the water window of several 100 eV and beyond (34-40) but applications with these sources up to now are scarce. For ultrafast applications, time-resolved photoelectron spectroscopy (PES) (41) with pump-probe schemes where the sample is pumped with a laser pulse and probed with HHG pulses at a defined pump-probe delay has emerged as a powerful tool for the investigation of ultrafast dynamics in gas phase samples (42-47) and on surfaces (48-54). A variety of set ups has been described to perform such experiments on gas phase samples (55-60), on surfaces (61-64) or on both (65, 66).

Inspired by the pioneering investigations of the groups of S. Leone, U. Heinzmann, M. Drescher, M. Murnane and H. Kapteyn (42, 52, 53, 65) we built a set up for time-resolved PES in the gas phase with HHG VUV pulses. We present here the details of two generations of the same set up and measurements to determine the spectral characteristics of the HHG source and the time resolution of the set up. The approach described here is based on HHG in a gas jet or cell with a grating monochromator to select one harmonic and is optimized for spectroscopic applications. This is in contrast to our alternative set up based on HHG in a capillary with selection of one harmonic with a transmission zone plate and aiming at microscopy applications (67).

We present in section II results on PES on gas phase samples with set up I (58) with HHG in a gas jet, without VUV focusing into the interaction region and with electron detection with an electrostatic hemispherical electron spectrometer to determine the bandwidth of our HHG source. In section III, results on femtosecond time-resolved PES where gas phase samples were pumped with optical laser pulses and probed with PES with

HHG VUV pulses are presented with set up II. In this second and current generation of the set up we perform HHG in a cell, focus the VUV radiation into the interaction region and use a magnetic bottle type time of flight electron spectrometer for PES. Side bands in the photoelectron spectra are used to determine the time resolution of the set up (68-79).

II. EXPERIMENTAL SET UP I AND RESULTS: SPECTRAL CHARACTERISTICS

A. Apparatus without VUV focusing

The first generation of our set up (set up I) is schematically drawn in Figure 1. In both generations of the set up, HHG is driven by a femtosecond Ti:sapphire laser system with a multipass amplifier with pulse energies of up to 2.5 mJ, a repetition rate of 1 kHz, typical pulse durations of 60 fs, and a center wavelength of 790 nm. This is the same laser system as it is used for the generation of femtosecond soft x-ray pulses at the electron storage ring BESSYII at the Helmholtz-Zentrum Berlin in the so called Femtoslicing facility (80, 81) and as we used it for driving an Optical Parametric Amplifier for time-resolved mid-infrared pump and soft x-ray absorption probe spectroscopy of liquid water with BESSYII (82, 83). Our HHG set up is thus located in the storage ring hall of BESSYII and approximately 8 m away from the Ti:saphhire laser system. We typically use pulse energies of 0.5-1.5 mJ for HHG and time-resolved experiments. The laser beam is split with a beamsplitter into pump and probe pulses (Fig. 1). In section II we shall only describe the probe part. The set up and results on pump-probe spectroscopy are presented in section III.

The first optical element we use in the probe part of the laser beam before generating high-order harmonics is a lambda-half plate. With this we align the polarization vector of the generated VUV radiation to be parallel with the orientation of the grooves in the grating of our toroidal monochromator to maximize the grating diffraction efficiency. This efficiency is maximized in our set up for the s-geometry with the polarization vector perpendicular to the diffraction plane.

Next we use a lens to focus the laser into the rare gas medium in the vacuum system for HHG. In set up I we used a gas jet as the HHG medium. The focal length of the lens, the laser pulse energy, the numerical aperture of the laser at the lens position, the length of the rare gas generation medium along the laser propagation axis and the gas medium pressure need to be optimized for a given generation gas to reach maximum VUV flux (1, 2, 4, 8-14). In our set up I we typically used focal lengths of 300-500 mm, pulse energies of 0.5-1 mJ, a

gas jet of 0.6 mm in diameter and a gas pressure (in the inlet tube) of several 10 mbar for Ar and Xe as generation gases and at a numerical aperture of the laser of 10-20 mm. The laser pulse energy was further optimized by adjusting the opening of a set of apertures to cut unwanted laser power and by optimizing the position of the jet with respect to the laser focus. The jet is typically placed slightly in front of the laser focus. The laser beam is coupled into the vacuum system through a glass window with anti-reflex coating. This window is placed as far away as possible from the laser focus to reduce the distortion of the laser wave front through non-linear processes in the window. The gas jet chamber is pumped with a turbo pump and the pressure was typically 10^{-2}-10^{-3} mbar when HHG was operated.

We use a toroidal grating monochromator ("LHT 30" from Jobin-Yvon) to select one harmonic in both generations of the set up. The grating has a toroidal surface with 550 grooves per mm (laminar profile) and is operated at a constant deviation angle of 142º. It is gold coated and has a calculated efficiency of 4-5% at 20 eV and 6-8% at 30 eV. The entrance and exit arms of the monochromator amount to 320 mm (distance between the slits and the rotation axis in the grating surface). The pressure in the monochromator is typically around 10^{-6} mbar when HHG is operated.

The toroidal grating images the entrance slit onto the exit slit. We note that the HHG source in our set ups is placed at a distance of 265 mm in front of the entrance slit. This introduces a slight astigmatism as the optimal position would be in the entrance slit. Ideally one would use an additional focusing mirror to image the HHG source onto the entrance slit. This concept is realized in a joint HHG set up for femtosecond spectroscopy between 20 and 100 eV with the group of M. Weinelt (Freie Universität Berlin, Germany) at the Max-Born-Institute (Berlin, Germany) (84). Besides the astigmatism, the short distance between the HHG source and the grating also prevents us from optimizing the so called "loose focusing conditions" of the driving laser for HHG in gas jets or cells (8, 9, 10, 11, 14) for optimal HHG flux as with a longer focal length the grating would be damaged by the driving laser. For the set ups described here we decided to accept these disadvantages as they turned out to be acceptable (see focus and flux measurements in section III). Furthermore, we minimized the distance between the HHG source and the grating in order to minimize these disadvantages and to minimize the number of illuminated grooves on the grating and, accordingly, minimize the temporal stretching of the femtosecond pulses. Finally, the realized optical layout bears a major advantage: Working without the additional VUV focusing element greatly facilitates the alignment of the set up.

Ray-tracing simulations (85) showed that at our comparably large monochromator exit slit size of 500 μm, one full harmonic is transmitted through the slit at photon energies of 20-30 eV. The PES measurements presented below hence reflect the bandwidth of the HHG source rather than the resolution of the monochromator. The ray-tracing simulations also showed that the expected pulse duration amounts to approximately 130 fs for a VUV beam divergence of 1 mrad (full width at half maximum, FWHM, see more details in section III for the measured pulse duration).

One crucial aspect in set ups for femtosecond VUV spectroscopy or imaging based on HHG is the suppression of the driving 790 nm laser after the HHG medium. This is particularly important if sensitive detectors such as VUV or x-ray charge-coupled devices (CCDs) are being used. Also for PES applications it is essential to ensure that no considerable amount of the driving laser reaches the sample area. This prevents photoionization of the sample itself or solid targets nearby the source volume of the electron spectrrometer such as a gas inlet by the remainder of the driving laser.

At typical conversion efficiencies of 10^{-6} to 10^{-7} for kHz laser systems with pulse energies of 1-2 mJ the power density from the driving laser that needs to be blocked can easily reach several W/cm^2. Often, it is sufficient to use a thin Al filter with a thickness of hundreds of nanometers to block most of the driving laser and to still have a high transmission for VUV radiation. More elaborate concepts have also been developed (86-88) and these are necessary in particular when an Al filter cannot dissipate the absorbed energy such as when the driving laser is only loosely focused and/or at high pulse energies. Here we use an Al filter of 150 nm thickness with a transmission of 70% at 20-30 eV (89) to block the driving laser. This filter is 1 inch in diameter and placed as far away as possible from the laser focus. We place it just in front of the monochromator grating at a distance of approximately 580 mm from the laser focus (Fig. 1). Care has to be taken to minimize oxidation of this Al filter as Al_2O_3 has a considerably lower transmission for VUV radiation than pure Al (70% at a thickness of 4 nm at 20-30 eV, ref. 89). We note that when the monochromator is run in first order to select one harmonic we do not need to place any Al filter into the beam as the remainder of the driving laser is diffracted away from the propagation axis of the selected harmonic and cannot reach the interaction region in the experimental chamber.

Between the exit slit of the monochromator and the experimental chamber (Fig. 1) we use a Au mesh and a diode mounted on a translational stage to measure and optimize the VUV flux once the laser propagation axis is properly aligned to the optical axis of the

monochromator. A calibrated GaAsP semiconductor photodiode (Hamamatsu model g112704) is used to measure the absolute photon flux. We confirmed in a cross-calibration measurement (90) with an absolute gas monitor detector for femtosecond VUV and x-ray pulses with high peak powers (91-93) that this diode yields reliable values for the femtosecond VUV flux of our HHG source within an uncertainty of ±15%.

A typical spectrum of our source with HHG in Ar gas is displayed in Fig. 2. This was measured by scanning the grating angle and recording the photocurrent generated on the Au mesh. The flux has been calibrated with the diode. The excellent spectral purity of our grating-based monochromator and the corresponding complete suppression of harmonics adjacent to the one selected for measurements is a key feature of the set up. It facilitates extracting weak transient signals in time-resolved PES as small photoelectron intensities within plus or minus 3.1 eV of strong main lines can be readily detected without worrying about a structured background due to photoionization from partially suppressed adjacent harmonics. In contrast, single multilayer mirrors (61) or pairs of multilayer mirrors (63, 66) were shown to transmit the adjacent harmonics with an intensity of the selected harmonic of 10% and more.

The VUV spot size in the interaction region in the experimental chamber in set up I amounted to approximately 1 mm in diameter. We did not use any VUV focusing device and we kept the flux at a comparably low level to prevent possible space charge effects in photoionization to accurately determine the bandwidth of our source from the width of photoelectron lines. The background pressure in the experimental chamber for PES is typically 2 x 10^{-8} mbar when HHG is operated and no further sample gas is introduced.

PES in set up I was performed with an electrostatic hemispherical electron energy analyzer (Scienta SES200). This electron spectrometer includes an electron lens system to parallelize the electron trajectories and to retard/accelerate the electrons to the fixed pass energy, a slit between the lens system and the hemisphere and an electron detector consisting of an MCP stack, a phosphor screen and a CCD camera. The resolution of this spectrometer has been extensively characterized (94, 95) and it can be easily controlled by changing the slit. The contribution of the spectrometer to the measured photoelectron line width (see section II B. and C.) is thus well known and this allows for accurate determination of the bandwidth of our HHG source. The sample gas for PES is introduced into the source volume of the electron spectrometer as an effusive gas jet through a simple gas inlet tube.

B. Photoelectron spectra for characterizing the bandwidth of the source

The results on PES of Xe and Ar as sample gases to determine the bandwidth of the HHG source with low flux (Ar generation) and high flux (Xe generation) are displayed in Figures 3 and 4, respectively. Note that the relative intensities of the lines in Fig. 3 (a) [the same holds for Fig. 4 (a) and Fig. 5] do not reflect the relative intensities of the respective harmonics as the photoelectron intensities also depend on the photoionization cross sections at the respective photon energies and the spectrum was not corrected for the varying transmission of the electron spectrometer. The sample gases were introduced into the interaction region until the pressure in the experimental chamber reached a value of 2-4 x 10^{-6} mbar.

The results on 5p photoionization of Xe as a sample gas with Ar as a generation gas are shown in Fig. 3. The spectra in first order were taken at a comparably low flux of ~10^8 photons/s (~10^5 photons/pulse at a repetition rate1 kHz) to rule out the influence of possible space charge effects. They were accumulated for 12 min [Fig. 3 (a)] and 23 min [Fig. 3 (b)]. Photoionization of the Xe 5p valence shell results in the final ionic states of Xe^+ [Kr] $5s^2$ $4d^{10}$ $5p^5$ with the two spin-orbit split final states Xe^+ $^2P_{3/2}$ and Xe^+ $^2P_{1/2}$ abbreviated as $5p_{3/2}$ and $5p_{1/2}$ in Fig. 3. Their binding energies amount to 12.1 and 13.4 eV (96), respectively. As these final states correspond to the ground states of the Xe^+ ion they can not further decay. With absent lifetime broadening the measured line widths thus directly represent the Gaussian instrumental broadening. In addition, the spin-orbit splitting of 1.3 eV is large enough to easily separate the two spin-orbit partners. The spectrum taken in first order selecting harmonic 13 at a photon energy 20.4 eV could be well fitted with two Gaussians and we find a FWHM of 220 meV [Fig. 3 (b)]. The fact that we measured the same width as in zero order of the monochromator (fit not shown) confirms our ray-tracing simulations and proves that the full harmonic is transmitted through the slit. Hence, the width of each line reflects the convolution of the bandwidth of the HHG source and the bandwidth of the electron spectrometer. Varying the flux by a factor of 10-20 by going from zero to first order in the monochromator has no effect on the measured line width and this shows that space charge effects are negligible. The electron spectrometer at the chosen settings (pass energy 20 eV, slit 4 mm) contributes to the line width with a broadening of approximately 150 meV (94, 95). We conclude that the bandwidth of our HHG source amounts to approximately 160 meV with an estimated uncertainty of ±30 meV. This is very similar to the 110±30 meV as determined for a similar set up by Nugent-Glandorf et al. (97). The background at low kinetic energies in Fig. 3 (a) is due to the fact that the VUV spot size was comparable to or larger

than the acceptance volume of the hemispherical electron energy analyzer projected along the VUV beam. It arises from electrons created at the borders of or outside the nominal acceptance volume of the electron analyzer. The intensity of this background strongly depends on the alignment of the VUV radiation with respect to the acceptance of the electron analyzer.

To further confirm the bandwidth measurement and to further test the possible influence of space charge effects we interchanged the sample and generation gases and repeated the measurement. The results on 3p photoionization of Ar as a sample gas with Xe as a generation gas are shown in Fig. 4. The spectra were taken at a flux approximately 50 times higher than in the former measurements and were accumulated for 2 min [Fig. 4 (a)] and 4 min [Fig. 4 (b)]. The final ionic states are Ar^+ [Ne] $3s^2$ $3p^5$ with the two spin-orbit split final states Ar^+ $^2P_{3/2}$ and Ar^+ $^2P_{1/2}$ [$3p_{3/2}$ and $3p_{1/2}$ in Fig. 4 with binding energies 15.7 and 15.9 eV (96), respectively]. Again, we could confirm that the full harmonic is transmitted through the slit (same width in zero order of the monochromator, fit not shown) and, with absent lifetime broadening, the measured line widths reflect the convolution of the HHG bandwidth and the bandwidth of the electron spectrometer. The spectrum taken with the 13^{th} harmonic (photon energy 20.4 eV) was fitted with two Gaussians with a FWHM of 200 meV [Fig. 4 (b)]. With the electron spectrometer contribution as for the former measurement (~150 meV) we conclude that the bandwidth of the HHG source amounted to approximately 130±30 meV. Reducing the flux in this measurement did not indicate any influence by space charge effects. The slight difference compared to the former measurement could hence be explained by the different generation conditions in Xe compared to Ar. Within error bars the results are very similar to the results reported by Nugent-Glandorf et al. (97).

We note that the comparably small bandwidth of around 150 meV is important for the application of the presented HHG set up for time-resolved PES as it facilitates the detection of weak transient signals when these approach the binding energies of photoelectron lines of un-pumped molecules (see section III C.).

C. VUV photoelectron spectroscopy of molecules in the gas phase

We present in Fig. 5 valence photoelectron spectra of gaseous CO_2 taken in set up I with Ar as a generation gas and in zero and first order of the monochromator. With a pressure of approximately 5 x 10^{-6} mbar in the experimental chamber and with accumulation times of

around 30 min for a spectrum in first order with 2 x 10^8 photons/s this shows that VUV photoelectron spectroscopy of molecules in the gas phase is easily feasible with a comparably simple set up based on HHG and even without focusing the HHG VUV radiation. In addition, Gaussian fits of the main photoelectron lines at a binding energy of 13.8 eV corresponding to the highest occupied molecular orbital (HOMO) in the CO_2 spectrum taken with harmonics 15 (23.6 eV), 17 (26.7 eV) and 19 (29.8 eV) (fits not displayed) show that the bandwidth of our source does not increase with increasing photon energy in the range considered here. We thus determine a value of 140 with an uncertainty of ±40 meV for the photon energies of 20-30 eV as used here (all uncertainties given here correspond to one standard error).

III. EXPERIMENTAL SET UP II AND RESULTS: TEMPORAL CHARACTERISTICS

A. Apparatus with VUV focusing

We now turn to the second and current generation of our set up (set up II, Fig. 6). Many components of set up II are the same as in set up I and we thus concentrate here on the differences and on what has not been described. Compared to set up I, in set up II the generation medium was changed from a jet to a cell, a mirror for focusing the HHG VUV radiation was added (corresponding measurements of the VUV focus are presented below), and the electron spectrometer was changed from an electrostatic hemispherical to a magnetic-bottle type time of flight spectrometer. In addition, set up II now also includes an ion time-of-flight spectrometer and we shortly describe here the pump-part of the Ti:sapphire laser beam.

In order to increase the transmission of the HHG VUV radiation in the generation-gas atmosphere in the generation chamber, to reduce the consumption of the generation gas for HHG and to reduce the load on the turbo pump on the generation chamber we replaced the jet by a cell. After again optimizing the focal length of the lens used to focus the laser beam into the cell, the laser pulse energy, the numerical aperture of the laser at the lens position, the thickness of the cell (length of the gas generation medium along the laser propagation axis) and the gas medium pressure, we derived an optimum cell thickness of 5 mm. The cell is about 1 inch x 1 inch in size and consists of a stainless steal holder with a feeding tube for the gas from the top and thin and easily renewable Cu foils right and left along the laser beam where the laser itself is used to drill holes with a size of tens of μm. We use a focal length of 500 mm at pulse energies of 0.5-1 mJ and at a numerical aperture of the laser of 20 mm, gas

pressures (measured approximately 200 mm away from the cell in the feeding) of 1-2 mbar for Ar and around 0.5 mbar for Xe. The pressure in the HHG chamber amounts to 2-6 x 10^{-3} mbar when HHG is operated. The background pressure in the experimental chamber for PES when HHG is operated is 2 x 10^{-8} mbar.

One of the disadvantages of set up I for time-resolved PES was the comparably large size of the VUV beam in the interaction region of the experimental chamber (1 mm in diameter). For pump-probe PES this meant that the pump-probe contrast or the ratio of pumped to un-pumped species was limited as the pump laser spot has to be of similar or ideally larger size than the VUV spot and this limited the pump-laser energy density. A consequence of this limited pump-probe contrast is the comparably weak side-band signal that we detected with set up I (58).

We thus installed in set up II a mirror for focusing the HHG VUV radiation (Fig. 6) with the aim to achieve a VUV spot size of around 100 μm and to enable higher pump-laser energy densities. This focusing mirror is mounted in a vacuum chamber with a 6-strut kinematical mount that allows for manually adjusting five axes independently from each other and without breaking the ultrahigh vacuum. Such a mount is essential to reach the best possible alignment of the mirror for the smallest focus. A schematic drawing of the optical layout of set up II and measured and simulated focal spots are shown in Fig. 7. The mirror images the exit slit of the monochromator to the interaction region in the experimental chamber with a demagnification of 2:1. It has a toroidal surface with Au coating on a fused silica substrate. The grazing angle is 6 º (measured from the surface) and the reflectivity was calculated to vary between 0.77 and 0.85 in the photon energy range between 20 and 100 eV. In the energy range of 20-30 eV used here its reflectivity amounts to 0.83. In order to keep aberrations small, the slope errors are limited to approximately 1” (both meridionally and sagitally) and the surface roughness was measured to be smaller than 5 Å.

The focusing capabilities of this mirror were characterized by mounting a back-thinned soft x-ray CCD camera in the nominal focal plane. We found a correlation between the measured shape of the focus and the divergence of the HHG VUV beam. The divergence was varied by baffling the beam. The corresponding measured focal spots are displayed in Figs. 7 (b)-(d). One can clearly see that the unwanted wings to the left of the focus can be avoided by reducing the divergence of the beam. In addition, we used this measurement to optimize the distance of the lens used to focus the laser into the generation cell [Figs. 7 (e)-(g)].

A comparison of the measured and simulated focal spots shows that most probably the wings were due to an over illumination of the focusing mirror. Care has thus to be taken to avoid generating a VUV beam with too high divergence. We found, though, that often when the divergence is large the flux is highest as well. For the best conditions for pump-probe measurements we thus typically trade in flux to reduce the divergence and check the size of the VUV beam in the interaction region with a Ce:YAG crystal on a regular basis. Depending on the details of the generation conditions and the quality of the alignment of the laser propagation axis to the optical axis of the VUV beam we estimate that we achieve, on a daily basis, focusing to approximately 100 μm horizontally and slightly less vertically [situation close to Figs. 7 (c) and (d)]. The astigmatism of the beam (see section II, due to the fact that the HHG source is 265 mm in front of the entrance slit of the toroidal monochromator) is apparent from the oval shape of the focal spot [Figs. 7 (c) and (d)].

We achieve a flux in set up II on a daily basis and with Xe as generation gas of approximately 10^{10} photons/s or 10^{7} photons/pulse in first order of the monochromator for 20.4 and 23.6 eV in the focus at the sample and in the measured bandwidth of 140 meV. With a combined transmission of 5% of the monochromator and the focusing mirror and with an estimated transmission of the Al filter of 15% due to an oxide layer of 10 nm on each side (8) we thus determine a flux from the source of ~1 x 10^{9} photons/pulse or ~3 nJ/pulse. For our pulse energies of the driving 790 nm laser of 0.5 mJ this corresponds to a conversion efficiency (based on the respective pulse energies) of 6 x 10^{-6}. This is similar to the conversion efficiencies reported in refs. (8) and (12) but lower by a factor of ~8 compared to ref. (14). We note that we report here values that we reach on a daily basis and without spending more than approximately 30 min to 1 hour in optimizing the flux on the sample before starting with the time-resolved PES experiments. The conversion efficiency could be possibly further optimized by more loosely focusing the driving laser but the short distance between the HHG source and the grating in our set up prevents us from doing this (see section II).

Another disadvantage of set up I was the low collection or detection efficiency of the electrostatic hemispherical electron analyzer of 1-2%. We thus built and installed in set up II a magnetic bottle type time of flight electron spectrometer. It is based on the design by Eland et al. (98) and was realized in cooperation with M. Meyer, who designed and built a similar spectrometer for PES applications at the free-electron laser FLASH in Hamburg (99). It is approximately 800 mm long and consists of meshes for retardation of the photoelectrons and a drift tube with a solenoid. A permanent magnet is used to reflect the half sphere opposite to

the drift tube into the spectrometer and electrons are detected with an MCP stack with a phosphor screen and, outside the vacuum system attached to a window flange, a photomultiplier tube (PMT). The PMT is used instead of a metal anode in order to be able to visually inspect the distribution of photoelectrons on the MCPs and to detect a possible asymmetry or misalignment. Commissioning measurements at the electron storage ring facility BESSYII showed that this spectrometer has a collection efficiency of 50-100% and, without retardation, an energy resolution of 2%. The retardation was tested for kinetic energies of up to 200 eV with retardation voltages of more than 150 V and, at least up to retardation voltages of 50 V, no considerable losses in collection efficiency were found. The increase in collection efficiency compared to the hemispherical spectrometer is essential in detecting weak transient signals in pump-probe PES as will be shown in section III C. The retardation is used to increase the resolution for the photoelectron lines under investigation and it turned out to be very useful for suppressing slow electrons arising from the pump-laser only. We additionally installed an ion time-of-flight spectrometer for characterizing the fragmentation of laser-pumped species.

Finally we shortly describe the pump-part of the Ti:sapphire laser in set up II (Fig. 6). We often use an 80:20 beamsplitter for probe:pump with pulse energies of 0.5-1 mJ for the probe and 0.4-0.2 mJ for the pump pulses, respectively. The pump pulses are delayed with a translational stage with a minimum step size of 1 μm. The polarization vector of the pump beam can be rotated with a lambda-half plate and we use a BBO crystal to convert 790 to 395 nm when needed. The pump-laser is focused into the interaction region with a lens with focal length of 400 mm. We typically focus the pump laser to a spot of approximately 200-400 μm in diameter in the interaction region. We use a fused silica viewport and a rectangular in-vacuum mirror that is placed just below the VUV beam to couple in the pump laser. Broadening of the time resolution due to the non-collinear in-coupling geometry is avoided by ensuring an angle of less than 1º between the pump and probe beams. Spatial overlap of pump and probe pulses is optimized with a Ce:YAG crystal that can be translated into the interaction region. We note that when the monochromator is run in zero order two instead of one Al filter are needed to block the remainder of the driving laser. Pump-probe time zero is first established by overlapping the 790 nm driving laser transmitted through the whole vacuum system and along the VUV path with the pump part behind the interaction region and outside the vacuum system. For this, we inspect the interference fringes on a video camera or we use a BBO crystal and generate 395 nm light when the two pulses overlap. In a second step the side band intensity in PES is used to optimize spatial overlap. Side bands (68) arise

from simultaneous absorption of VUV-probe and laser-pump photons when both pulses overlap in time and space. They are expressed in the photoelectron spectra as additional lines shifted in kinetic energy with respect to the main photoelectron lines by the energy of one or more pump-laser photons. Side bands have been extensively used in the past to either characterize the temporal characteristics of femtosecond VUV sources or to answer specific scientific questions in PES from gas phase samples and from surfaces (49, 55, 69-79).

B. Photoelectron spectra for characterizing the temporal resolution of the set up

We present in Figs. 8 and 9 time-resolved PES measurements on Ar as a sample gas with a laser-pump wavelength of 790 nm and HHG VUV probing in zero and first order of the monochromator. All spectra were taken without retardation voltage on the time-of-flight electron spectrometer and with Ar as a generation gas. The Ti:sapphire laser pulse energies used for pump and probe amounted to approximately 0.3-0.2 and 0.7-0.8 mJ, respectively.

Ar 3p photoelectron intensities taken in zero order of the monochromator are displayed versus electron flight time, kinetic energy and delay time between pump and probe pulses in Fig. 8 (a). One clearly sees the side bands between the main Ar 3p photoelectron lines at energies shifted by the energy of the pump photon energy of ±1.56 eV and the depletion and a Stark shift of the main lines when the two pulses overlap in time. This map was measured at a pressure in the experimental chamber of 5 x 10^{-7} mbar with an accumulation time of 30 s/delay step. With a total of 22 steps the accumulation time amounts to 11 min for the whole map. The integrated intensity of the side band at 328 ns flight time (15.6 eV kinetic energy) is plotted in Fig. 8 (b) and fitted with a Gaussian with a FWHM of 90 fs. This represents a cross-correlation measurement of pump and probe pulses. With a pulse duration of 60 fs of the 790 nm Ti:sapphire driving pulses we determine a similar pulse duration of the VUV probe pulses in zero order of the monochromator of 60-70 fs. The spectra in Fig. 8 (c) compare the situation for overlapping pulses and without pump laser. They were taken in zero order of the monochromator and accumulated for 50 s each. They show that the side band intensity can be even larger than the main line intensities. A fit of the main lines at kinetic energies of 4.5 eV and 17 eV with each two Gaussian profiles for the two spin-orbit split partners Ar $3p_{1/2}$ and $3p_{3/2}$ reveals a FWHM of 180 meV and 410 meV, respectively. With the bandwidth of the source of ~140 meV we thus determine a resolution

of our magnetic bottle type time of flight electron spectrometer of ~110 meV and ~380 meV at kinetic energies of 4.5 and 17 eV.

Ar 3p photoelectron intensities taken in first order of the monochromator with the 21st harmonic (33 eV) are displayed versus kinetic energy and delay time in Fig. 9 (a). The side bands at ±1.56 eV with respect to the kinetic energy of the main line and the concurrent main line depletion are clearly discernible. This series of spectra was measured at a pressure in the experimental chamber of 5 x 10^{-7} mbar with an accumulation time of 200 s/delay step. With a total of 22 steps the accumulation time of this series amounts to 73 min. The integrated intensity of the side band at higher kinetic energy is plotted in Fig. 9 (b) and fitted with a Gaussian with a FWHM of 135 fs (uncertainty ±5 fs). This is a cross-correlation measurement of pump and probe pulses in first order of the monochromator and includes the VUV pulse stretching of the monochromator grating. With a pulse duration of 60 fs of the 790 nm Ti:sapphire driving pulses we determine a pulse duration of the VUV probe pulses in first order of the monochromator of 120 fs in good agreement with our estimation based on a ray-tracing simulation (see section II A.). We did not find any evidence for varying pulse durations in the photon range of 20 to 30 eV.

This comparably short pulse duration for monochromatized HHG VUV pulses makes our set up unique in a sense that, to the best of our knowledge, this is the shortest pulse duration measured so far with a monochromator based on a single grating. Shorter femtosecond pulses have been produced with pairs of multilayer optics (57, 63, 66) and pairs of gratings mounted in conical diffraction (55, 56). Compared to other set ups based on conventional diffraction gratings (60) we produce shorter pulses because the grazing angle on the grating is comparably large and the distance of the HHG source to the grating is very short. We show in section III C. that a pulse duration of 120 fs is sufficient to efficiently measure the valence photoelectron evolution during molecular dissociation of Br_2. Still, we plan to mount a new grating with only 200 grooves/mm in our set up II. This should yield the same spectral purity as the grating we are using now but with pulse durations of around 70 fs.

The spectra in Fig. 9 (c) for overlapping pulses and without pump laser were accumulated in first order with harmonic 19 (29.8 eV) and for 800 s each. They show that we can observe up to eight side bands where the eighth side band corresponds to the simultaneous absorption of one VUV and eight 790 nm pump laser photons.

C. Femtosecond VUV photoelectron spectroscopy of molecules in the gas phase

In order to illustrate the capabilities of our set up II we present time-resolved valence photoelectron spectra of dissociating Br_2 molecules in Figs. 10 and 11. Details of this experiment can be found in ref. (45). The Br_2 molecules were excited by single-photon absorption at 395 nm by frequency-doubling the fundamental with the BBO crystal in the pump beam. This electronic excitation to the Br_2^* ($^1\Pi_u$) dissociative state leads to dissociation in two ground-state Br atoms. We used 790 nm laser-pump energies of 300 μJ to generate 30 μJ at 395 nm (power density less than 10^{12} W/cm^2). The laser pulse energy in the probe part of the beam was 1 mJ and we used Xe as a generation gas. The spectra were taken with the 15th harmonic (23.6 eV) at a HHG VUV flux of 5 x 10^9 photons/s. We used a retardation voltage of 7 V at the magnetic bottle type time of flight electron spectrometer. The combined kinetic-energy resolution resulting from the convolution of the bandwidth of the source and the resolution of the electron spectrometer amounted to 150 meV for kinetic energies of less than ~6 eV (resolution dominated by the bandwidth of the VUV pulses) and 250 meV for 6-9 eV (resolution given by the approximately equal bandwidths of the VUV pulses and the resolution of the electron spectrometer). The pressure in the experimental chamber was set to 5 x 10^{-7} mbar and data were accumulated for 2000 s for each delay step. With a total of 13 delay steps the accumulation time of the whole data set amounted to 7 hours and 13 min. The photoelectron spectra in Fig. 10 display the signatures of the un-pumped Br_2 molecules (molecular states X, A and B, note the depleting intensity), the photoelectron lines of the free Br atoms with the multiplet components ^{3}P, ^{1}D and ^{1}S, as well as the side bands. The count rates were 3-20 counts/s for the un-pumped main lines, up to 2 counts/s for the free atom lines and up to 1 count/s for the side bands. These results clearly show that an excellent spectral purity of the HHG photon source with a bandwidth in the order of hundreds of meV or less are needed to detect the details of the electronic structure during molecular dissociation in the gas phase in particular when transient features show up close to the binding energies of the lines of un-pumped species (Fig. 11). The evolution of the photoelectron spectrum of photoexcited Br_2 in the binding energy region of the atomic ^{3}P multiplet from the spectrum of the excited molecule with states A' and B' at early delays to the spectrum of the free atom with the $^2P_2$ and $^3P_{1,\,0}$ lines is shown in Fig. 11 (a). A broad intensity distribution characteristic of the transient molecular A' and B' states evolves into the comparably sharp lines of the free atom within less than 100 fs. Clearly, a time resolution of 135 fs or less with HHG VUV pulse durations of 120 fs is needed to follow this evolution in time. The evolution of all valence states from photoexcited molecules to the free atom is

shown as measured in Fig. 11 (b) and as calculated in Fig. 11 (c) (45). In order to follow all valence states with time and to accurately determine the dissociation time (45) it turned out to be essential to also detect the weak transient molecular states A' and B' at early delays and to clearly separate them from the atomic lines that occur at later delays. The count rate of the transient A' and B' signals at early times was as low as 0.1 count/s [Fig. 11 (a), delay -17 fs] and this clearly demonstrates that a maximum possible detection efficiency for the photoelectrons is needed for such experiments. The maps displaying the evolution of all valence states from photoexcited molecules to the free atoms in Figs. 11 (b) and (c) furthermore illustrate that in order to follow the valence states with time an optimal combination of a short pulse duration and a small bandwidth is needed. Too long pulses would broaden the features in the vertical while pulses with a large bandwidth (such as pulses with attosecond duration) would broaden the features along the horizontal direction in this map.

IV. SUMMARY

In our laser-based tabletop approach to femtosecond time-resolved photoelectron spectroscopy with photons in the VUV energy range we produce fs pulses by HHG of an amplified femtosecond Ti:sapphire laser system at a repetition rate of 1 kHz. Two generations of the same set up and results from photoelectron spectroscopy in the gas phase are discussed. A toroidal grating monochromator was used in both generations of the set up to select one harmonic in the energy range of 20-30 eV. With the first generation of the set up (set up I), where we produced HHG VUV photons in a gas jet, we performed photoelectron spectroscopy in the gas phase without focusing the HHG VUV radiation after the monochromator and determined the bandwidth of the source.from the width of Xe 5p and Ar 3p photoelectron lines. We find that one full harmonic is transmitted through the slit of our monochromator and with the known contribution of the electrostatic hemispherical electron spectrometer we find that our HHG source has a bandwidth of 140±40 meV. The second and current generation of the set up (set up II) is optimized for femtosecond pump-probe photoelectron spectroscopy with high flux and high brilliance of the femtosecond probe pulses generated in a cell. The HHG VUV pulses in this set up are focused into the interaction region with a toroidal mirror and the presented measurements of the focal spot indicate that we focus the HHG VUV radiation to a spot smaller than 100 x 100 μm^2. The

flux amounts to 10^{10} photons/s at the sample with Xe as a generation gas. Compared to set up I we increased the electron detection efficiency by installing a magnetic bottle time of flight electron spectrometer. Results on laser-pump HHG VUV probe PES show that the duration of the monochromatized VUV pulses is 120 fs resulting in an overall pump-probe time resolution of 135±5 fs, as determined from measuring side band intensities in rare gas photoelectron spectra. We finally show how this set up can be used to map the transient valence electronic structure in molecular dissociation of Br_2 in the gas phase. The importance of combining HHG VUV pulses with both a short duration and a small bandwidth as well as the high detection efficiency for the photoelectrons in order to detect weak transient signals are highlighted.

Acknowledgments

J.G. acknowledges support by the European Union Marie Curie program. We thank P. Zimmermann for providing the hemispherical electron spectrometer and S. Eisebitt for providing the soft x-ray CCD camera. We gratefully acknowledge M. Meyer for collaboration on the design of the magnetic bottle type time of flight electron spectrometer and J. Viefhaus for support with the commissioning measurements of the spectrometer. We are grateful to the BESSYII staff for continuous assistance and in particular to R. Mitzner, T. Quast, J.-S. Schmid, and G. Reichardt.

References

1. T. Pfeifer, C. Spielmann, G. Gerber, Rep. Prog. Phys. **69**, 443 (2006).

2. T. Popmintchev, M.-C. Chen, P. Arpin, M. Murnane, H. Kapteyn, Nature Photonics **4**, 822 (2010).

3. F. Krausz, M. Ivanov, Rev. Mod. Phys. **81**, 163 (2009).

4. L. Van Dao, S. Teichmann, J. Davis, P. Hannaford, J. Appl. Phys. **104**, 023105 (2008).

5. J. Hüve, T. Haarlammert, T. Steinbrück, J. Kutzner, G. Tsimilis, H. Zacharias, Optics Communications **266**, 261 (2006).

6. A. Flettner, J. Günther, M. B. Mason, U. Weichmann, R. Düren, G. Gerber, Appl. Phys. B **73**, 129 (2001).

7. G. Sommerer, E. Mevel, J. Hollandt, D. Schulze, P. V. Nickles, G. Ulm, W. Sandner, Optics Communications **146**, 347 (1998).

8. X. He, M. Miranda, J. Schwenke, O. Guilbaud, T. Ruchon, C. Heyl, E. Georgadiou, R. Rakowski, A. Persson, M. B. Gaarde, A. L'Huillier, Phys. Rev. A **79**, 063829 (2009).

9. J.-F. Hergott, M. Kovacev, H. Merdji, C. Hubert, Y. Mairesse, E. Jean, P. Berger, P. Agostini, B. Carré, P. Salières, Phys. Rev. A **66**, 021801(R) (2002).

10. E. Takahashi, Y. Nabekawa, T. Otsuka, M. Obara, K. Midorikawa, Phys. Rev. A **66**, 021802(R) (2002).

11. C. Delfin, A. Altucci, F. De Filippo, C. de Lisio, M. B. Gaarde, A. L'Huillier. L. Roos, C.-G. Wahlström, J. Phys. B : At. Mol. Opt. Phys. **32**, 5397 (1999).

12. M. Schnürer, Z. Cheng, M. Hentschel, G. Tempea, P. Kálmán, T. Brabec, F. Krausz, Phys. Rev. Lett. **83**, 722 (1999).

13. Y. Tamaki, J. Itatani, Y. Nagata, M. Obara, K. Midorikawa, Phys. Rev. Lett. **82**, 1422 (1999).

14. E. Constant, D. Garzella, P. Berger, E. Mével, Ch. Dorrer, C. Le Blanc, F. Salin, P. Agostini, Phys. Rev. Lett. **82**, 1668 (1999)

15. A. Rundquist, C. G. Durfee, Z. Chang, C. Herne, S. Backus, M. M. Murnane, H. C. Kapteyn, Science **280**, 1412 (1998).

16. T. Haarlammert, H. Zacharias, Current Opinion in Solid State and Materials Science **13**, 13 (2009).

17. M. Bauer, J. Phys. D: Appl. Phys. **38**, R253 (2005).

18. W. Li, A. A. Jarón-Becker, C. W. Hogle, V. Sharma, X. Zhou, A. Becker, H. C. Kapteyn, M. M. Murnane, PNAS **107**, 20219 (2010).

19. H. J. Wörner, J. B. Bertrand, D. V. Kartashov, P. B. Corkum, D. M. Villeneuve, Nature **466**, 604 (2010).

20. H. Soifer, P. Botheron, D. Shafir, A. Diner, O. Raz, B. D. Bruner, Y. Mairesse, B. Pons, N. Dudovich, Phys. Rev. Lett. **105**, 143904 (2010).

21. K. R. Siefermann, Y. Liu, E. Lugovoy, O. Link, M. Faubel, U. Buck, B. Winter, B. Abel, Nature Chem. **2**, 274 (2010).

22. C. La-O-Vorakiat, M. Siemens, M. M. Murnane, H. C. Kapteyn, S. Mathias, M. Aeschlimann, P. Grychtol, R. Adam, C. M. Schneider, J. M. Shaw, H. Nembach, T. J. Silva, Phys. Rev. Lett. **103**, 257402 (2009).

23. Z.-H. Loh, S. R. Leone, J. Chem. Phys. **128**, 204302 (2008).

24. Y. Mairesse, D. Zeidler, N. Dudovich, M. Spanner, J. Levesque, D. M. Vielleneuve, P. B. Corkum, Phys. Rev. Lett. **100**, 143903 (2008).

25. E. Seres, C. Spielmann, Appl. Phys. Lett. **91**, 121919 (2007).

26. E. Gagnon, P. Ranitovic, X.-M. Tong, C. L. Cocke, M. M. Murnane, H. C. Kapteyn, A. S. Sandhu, Science **317**, 1374 (2007).

27. T. Shimizu, T. Sekikawa, T. Kanai, S. Watanabe, M. Itoh, Phys. Rev. Lett. **91**, 017401 (2003).

28. R. Früke, J. Kutzner, T. Wittig, H. Zacharias, Th. Wilhein, Europhy. Lett. **72**, 915 (2005).

29. M. Wieland, C. Spielmann, U. Kleineberg, Th. Westerwalbesloh, U. Heinzmann, T. Wilhein, Ultramicroscopy **102**, 93 (2005).

30. A. Ravasio, D. Gauthier, F. R. N. C. Maia, M. Billon, J.-P. Caumes, D. Garzella, M. Géléoc, O. Gobert, J.-F. Hergott, A.-M. Pena, H. Perez, B. Carré, E. Bourhis, J. Gierak, A. Madouri, D. Mailly, B. Schiedt, M. Fajardo, J. Gautier, P. Zeitoun, P. H. Bucksbaum, J. Hajdu, H. Merdji, Phys. Rev. Lett. **103**, 028104 (2009).

31. R. L. Sandberg, C. Song, P. W. Wachulak, D. A. Raymondson, A. Paul, B. Amirbekian, E. Lee, A. E. Sakdinawat, C. La-O-Vorakiat, M. C. Marconi, C. S. Menoni, M. M. Murnane, J. J. Rocca, H. C. Kapteyn, J. Miao, PNAS **105**, 24 (2008).

32. G. Genoud, O. Guilbaud, E. Mengotti, S.-G. Pettersson, E. Georgiadou, E. Pourtal, C.-G. Wahlström, A. L'Huillier, Appl. Phys. B, DOI 10.1007/s00340-007-2898-x (2008).

33. R. L. Sandberg, A. Paul, D. A. Raymondson, S. Hädrich, D. M. Gaudiosi, J. Holtsnider, R. I. Tobey, O. Cohen, M. M. Murnane, H. C. Kapteyn, Phys. Rev. Lett. **99**, 098103 (2007).

34. M.-C. Chen, P. Arpin, T. Popmintchev, M. Gerrity, B. Zhang, M. Seaberg, D. Popmintchev, M. M. Murnane, H. C. Kapteyn, Phys. Rev. Lett. **105**, 173901 (2010).

35. E. J. Takahashi, T. Kanai, K. L. Ishikawa, Y. Nabekawa, K. MIdorikawa, Phys. Rev. Lett. **101**, 253901 (2008).

36. D. M. Gaudiosi, B. Reagan, T. Popmintchev, M. Grisham, M. Barrill, O. Cohen, B. C. Walker, M. M. Murnane, H. C. Kapteyn, J. J. Rocca, Phys. Rev. Lett. **96**, 203001 (2006).

37. J. Seres, E. Seres, A. J. Verhoef, G. Tempea, C. Streli, P. Wobrauschek, V. Yakovlev, A. Scrinzi, C. Spielmann, F. Krausz, Nature **433**, 596 (2005).

38. E. Seres, J. Seres, F. Krausz, C. Spielmann, Phys. Rev. Lett. **92**, 163002 (2004).

39. E. A. Gibson, A. Paul, N. Wagner, R. Tobey, S. Backus, I. P. Christov, M. M. Murnane, H. C. Kapteyn, Phys. Rev. Lett. **92**, 033001 (2004).

40. E. A. Gibson, A. Paul, N. Wagner, R. Tobey, D. Gaudiosi, S. Backus, I. P. Christov, A. Aquila, E. M. Gullikson, D. T. Attwood, M. M. Murnane, H. C. Kapteyn, Science **302**, 95 (2003).

41. Stolow, A., Bragg, A. E., & Neumark, D. M., Chem. Rev. **104**, 1719 (2004).

42. L. Nugent-Glandorf, M. Scheer, D. A. Samuels, A. M. Mulhisen, E. R. Grant, X. Yang, V. M. Bierbaum, S. R. Leone, Phys. Rev. Lett. **87**, 193002 (2001).

43. L. Nugent-Glandorf, M. Strasser, D. A. Samuels, V. M. Bierbaum, S. R. Leone, J. Chem. Phys. **117**, 6108 (2002).

44. D. Strasser, F. Goulay, and S. R. Leone, J. Chem. Phys. **127**, 184305 (2007).

45. Ph. Wernet, M. Odelius, K. Godehusen, J. Gaudin, O. Schwarzkopf, W. Eberhardt, Phys. Rev. Lett. **103**, 013001 (2009).

46. L. H. Haber, B. Doughty, S. R. Leone, Phys. Rev A **79**, 031401(R) (2009).

47. D. Strasser, T. Pfeifer, B. J. Hom, A. M. Müller, J. Plenge, S. R. Leonem Phys. Rev. A **73**, 021805(R) (2006).

48. A. Melzer, D. Kampa, J. Wang, T. Fauster, Phys. Rev. B **80**, 205424 (2009).

49. L. Miaja-Avila, G. Saathoff, S. Mathias, J. Yin, C. La-o-vorakiat, M. Bauer, M. Aeschlimann, M. M. Murnane, H. C. Kapteyn, Phys. Rev. Lett. **101**, 046101 (2008).

50. S. Guizard, A. N. Belsky, J. Gaudin, G. Geoffroy, Pa. Martin, G. Petite, A. Philippov, B. N. Yatsenko, Phys. Stat. Sol. C **2**, 233 (2005).

51. C. Lei, M. Bauer, K. Read, R. Tobey, Y. Liu, T. Popmintchev, M. M. Murnane, H. C. Kapteyn, Phys. Rev. B **66**, 245420 (2002).

52. P. Siffalovic, M. Drescher, and U. Heinzmann, Europhys. Lett. **60**, 924 (2002).

53. M. Bauer, C. Lei, K. Read, R. Tobey, J. Gland, M. M. Murnane, H. C. Kapteyn, Phys. Rev. Lett. **87**, 025501 (2001).

54. K. Read, H. S. Karlsson, M. M. Murnane, H. C. Kapteyn, R. Haight, J. Appl. Phys. **90**, 294 (2001).

55. M. Ito, Y. Kataoka, T. Okamoto, M. Yamashita, T. Sekikawa, Optics Express **18**, 6071 (2010).

56. L. Poletto, P. Villoresi, F. Frassetto, F. Calegari, F. Ferrari, M. Lucchini, G. Sansone, M. Nisoli, Rev. Sci. Instrum. **80**, 123109 (2009).

57. E. Gagnon, A. S. Sandhu, A. Paul, K. Hagen, A. Czasch, T. Jahnke, P. Ranitovic, C. L. Cocke, B. Walker, M. M. Murnane, H. C. Kapteyn, Rev. Sci. Instrum. **79**, 063102 (2008).

58. Ph. Wernet, K. Godehusen, O. Schwarzkopf, W. Eberhardt, Ultrafast Phenomena XV, Springer Series in Chemical Physics **88**, 45 (2007).

59. K. Oguri, T. Ozaki, T. Nishikawa, H. Nakano, Appl. Phys. B **78**, 157 (2004).

60. L. Nugent-Glandorf, M. Strasser, D. A. Samuels, V. Bierbaum, S. R. Leone, Rev. Sci. Instrum. **73**, 1875 (2002).

61. G. L. Dakovski, Y. Li, T. Durakiewicz, G. Rodriguez, Rev. Sci. Instrum. **81**, 073108 (2010).

62. B. H. Christensen, M. K. Raarup, P. Balling, Nuclear Instruments and Methods in Physics Research A **615**, 114 (2010).

63. S. Mathias, L. Miaja-Avila, M. M. Murnane, H. C. Kapteyn, M. Aeschlimann, M. Bauer, Rev. Sci. Instrum. **78**, 083105 (2007).

64. G. Tsilimis, C. Benesch, J. Kutzner, H. Zacharias, J. Opt. Soc. Am. B **20**, 246 (2003).

65. M. Drescher, P. Siffalovic, M. Spieweck, U. Heinzmann, Journal of Electron Spetrocopy and Related Phenomena **127**, 103 (2002).

66. P. Siffalovic, M. Drescher, M. Spieweck, T. Wiesenthal, Y. C. Lim, R. Weidner, A. Elizarov, U. Heinzmann, Rev. Sci. Instrum. **72**, 30 (2001).

67. J. Gaudin, S. Rehbein, P. Guttmann, S. Godé, G. Schneider, Ph. Wernet, W. Eberhardt, J. Appl. Physics **104**, 033112 (2008).

68. T. E. Glover, R. W. Schoenlein, A. H. Chin, C. V. Shank, Phys. Rev. Lett. **76**, 2468 (1996).

69. L. H. Haber, B. Doughty, S. R. Leone, Molecular Physics **108**, 1241 (2010).

70. L. H. Haber, B. Doughty, S. R. Leone, J. Phys. Chem. A **113**, 13152 (2009).

71. G. Saathoff, L. Miaja-Avila, M. Aeschlimann, M. M. Murnane, H. C. Kapteyn, Phys. Rev. A **77**, 022903 (2008).

72. P. Radcliffe, S. Düsterer, A. Azima, H. Redlin, J. Feldhaus, J. Dardis, K. Kavanagh, H. Luna, J. Pedregosa Gutierrez, P. Yeates, E. T. Kennedy, J. T. Costello, A. Delserieys, C. L. S. Lewis, R. Taieb, A. Maquet, D. Cubaynes, M. Meyer, Appl. Phys. Lett. **90**, 131108 (2007).

73. L. Maija-Avila, C. Lei, M. Aeschlimann, J. L. Gland, M. M. Murnane, H. C. Kapteyn, G. Saathoff, Phys. Rev. Lett. **97**, 113604 (2006).

74. J. Mauritsson, P. Johansson, R. López-Martens, K. Varjú, A. L'Huillier, M. B. Gaarde, K. J. Schafer, J. Phys. B : At. Mol. Opt. Phys. **38**, 2265 (2005).

75. P. O'Keeffe, R. López-Martens, J. Mauritsson, A. Johansson, A. L'Huillier, V. Véniard, R. Taieb, A. M aquet, M. Meyer, Phys. Rev. A **69**, 051401(R) (2004).

76. R. López-Martens J. Mauritsson, A. Johansson, J, Norin, A. L'Huillier, Eur. Phys. J. D **26**, 105 (2003).

77. J. Norin, J. Mauritsson, A. Johansson, M. K. Raarup, S. Buil, A. Persson, O. Dühr, M. B. Gaarde, K. J. Schafer, U. Keller, C.-G. Wahlström, A. L'Huillier, Phys. Rev. Lett. **88**, 193901 (2002).

78. E. S. Toma, H. G. Muller, P. M. Paul, P. Berger, M. Cheret. P. Agostini, C. Le Blanc, G. Mullot, G. Cheriaux, Phys. Rev. A **62**, 061801(R) (2000).

79. A. Bouhal, R. Evans, G. Grillon, A. Mysyrowicz, P. Berger, P. Agostini, R. C. Constantinescu, H. G. Muller, D. von der Linde, J. Opt. Soc. Am. B **14**, 950 (1997).

80. S. Khan, K. Holldack, T. Kachel, R. Mitzner, T. Quast, Phys. Rev. Lett. **97**, 074801 (2006).

81. K. Holldack, S. Khan, R. Mitzner, T. Quast, Phys. Rev. Lett. **96**, 054801 (2006)

82. G. Gavrila, K. Godehusen, C. Weniger, E. T. J. Nibbering, T. Elsaesser, W. Eberhardt, Ph. Wernet, Appl. Phys. A **96**, 11 (2009).

83. Ph. Wernet, G. Gavrila, K. Godehusen, C. Weniger, E. T. J. Nibbering, T. Elsaesser, W. Eberhardt, Appl. Phys. A **92**, 511 (2008).

84. http://www.mbi-berlin.de/de/research/projects/4-1/subprojects/UP3/main.htm

85. F. Schäfers, RAY - THE BESSY RAYTRACE PROGRAM, In: Springer Series in Modern Optical Sciences: Modern Developments in X-Ray and Neutron Optics, Eds. A. Erko, M. Idir, Th. Krist, A.G. Michette, Springer Berlin/Heidelberg, Vol. 137, 9-41 (2008).

86. R. Hörlein, Y. Nomura, J. Osterhoff, Zs. Major, S. Karsch, F. Krausz, G. D. Tsakiris, Plasma Phys. Control. Fusion **50**, 124002 (2008).

87. Y. Nagata, Y. Nabekawa, K. Midorikawa, Optics Letters **31**, 1316 (2006).

88. E. J. Takahashi, H. Hasegawa, Y. Nabekawa, K. Midorikawa, Optics Letters **29**, 507 (2004).

89. B. Henke, E. Gullikson, J. Davis J., Atomic Data and Nuclear Data Tables **54**, 181 (1993).

90. T. Leitner, A. A. Sorokin, J. Gaudin, H. Schoeppe, K. Tiedtke, M. Richter, W. Eberhardt, Ph. Wernet, submitted (2010).

91. M. Richter, A. Gottwald, U. Kroth, A. Sorokin, S. Bobashev, L. Shmaenok, J. Feldhaus, Ch. Gerth, B. Steeg, K. Tiedtke, R. Treusch, Appl. Phys. Lett. **83**, 2970 (2003).

92. K. Tiedtke, J. Feldhaus, U. Hahn, U. Jastrow, T. Nunez, T. Tschentscher, S. Bobashev, A. Sorokin, J. Hastings, S. Moller, L. Cibik, A. Gottwald, A. Hoehl, U. Kroth, M. Krumrey, H. Schoeppe, G. Ulm, M. Richter, J. Appl. Phys. **103**, 094511 (2008).

93. N. Saito, P. Juranic, M. Kato, M. Richter, A. Sorokin, K. Tiedtke, U. Jastrow, U. Kroth, H. Schoeppe, M. Nagasono, M. Yabashi, K. Tono, T. Togashi, H. Kimura, H. Ohashi, T. Ishikawa, Metrologia **47**, 21 (2010).

94. Ph. Wernet, Dilpomarbeit, Universität Hamburg (1997).

95. W. Benten, Diplomarbeit, Technische Universität Berlin (1997).

96. K. Kimura, S. Katsumata, Y. Achiba, T. Yamazaki, S. Iwata, Hendbook of HeI Photoelectron Spetra of Fundamental Organic Molecules, Japan Scientific Societies Press, Tokyo, Halsted Press, New York (1980).

97. L. Nugent-Glandorf, M. Strasser, M. Krishnamurthy, J. W. Odom, S. R. Leone, Phys. Rev. A **62**, 023812 (2000).

98. J. Eland, O. Vieuxmaire, T. Kinugawa, P. Lablanquie, R. Hall, F. Penent, Phys. Rev. Lett. **90**, 530031 (2003).

99. P. Radcliffe, S. Düsterer, A. Azima, W. B. Li, E. Plönjes, H. Redin, J. Feldhaus, P. Nicolosi, L. Poletto, J. Dardis, J. P. Gutierrez, P. Hough, K. D. Kavanagh, E. T. Kennedy, H. Luna, P. Yeates, J. T. Costello, A. Delyseries, C. L. S. Lewis, D. Glijer, D. Cubaynes, M. Meyer, Nuclear Instruments and Methods in Physics Research A **583**, 516 (2007).

Figures

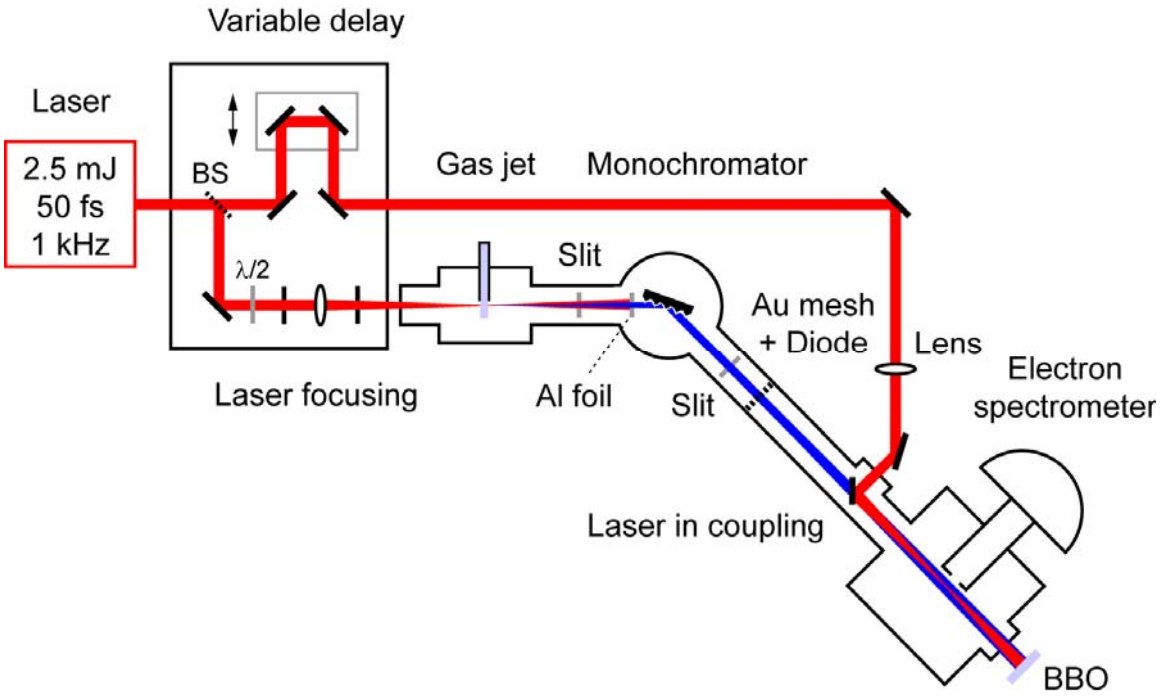

Figure 1: Schematic representation of the experimental set up (set up I) with generation of the femtosecond high-order harmonics in a gas jet, without VUV focusing and with a hemispherical electron spectrometer. BS denotes the beamsplitter and λ/2 the lambda half plate in the probe part of the laser beam.

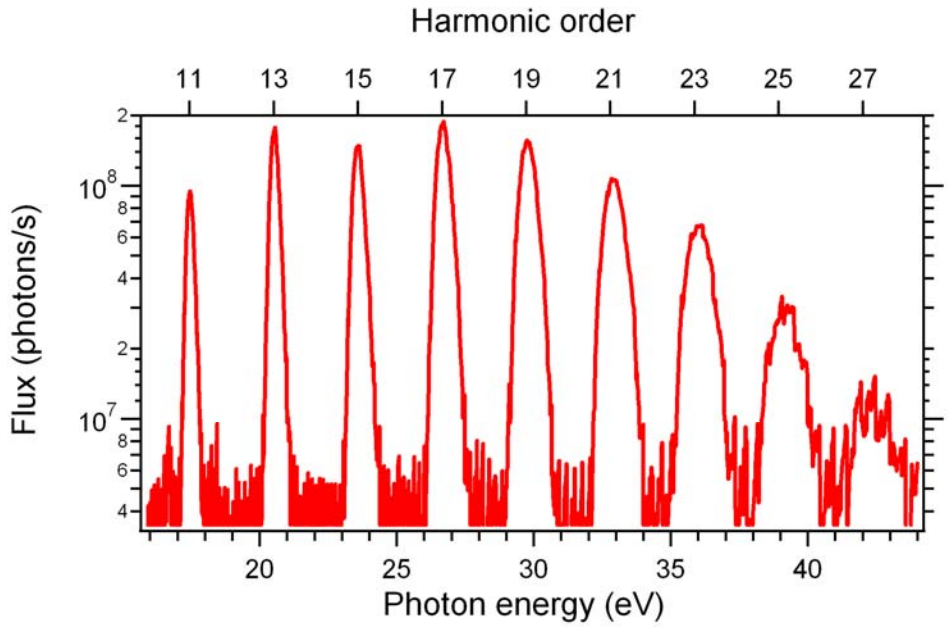

Figure 2: High-order harmonic generation spectrum and flux at the sample for set up I measured at 1 kHz repetition rate with Ar as generation gas. The flux for pump-probe experiments with set up II was typically chosen to be up to one order of magnitude higher.

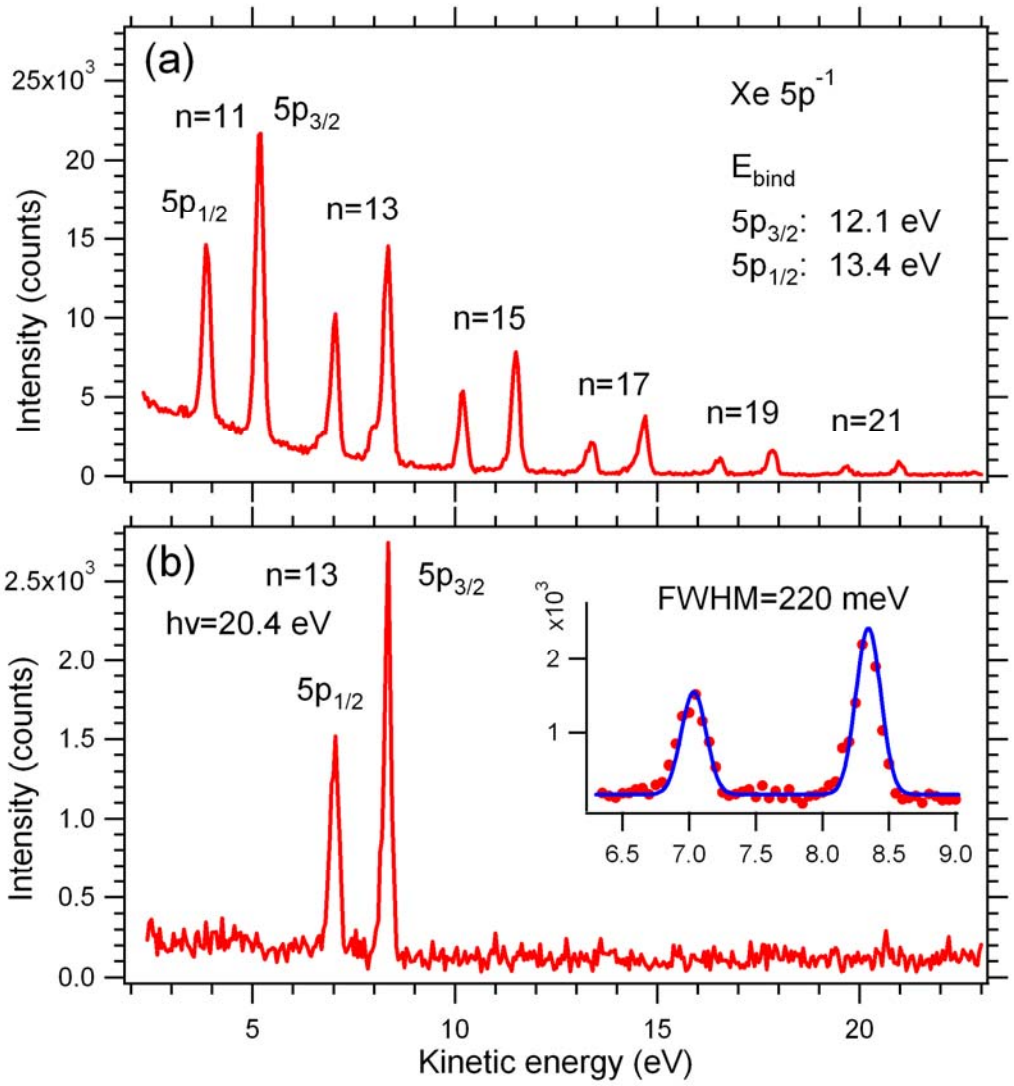

Figure 3: 5p photoelectron spectra of Xe as a sample gas with the two spin-orbit split lines $5p_{1/2}$ and $5p_{3/2}$ taken in set up I with Ar as a generation gas and with the monochromator in zero order in (a) and in first order (selecting the 13th harmonic at 20.4 eV) in (b). In the inset in (b) a fit (blue line with two Gaussian profiles with FWHM of 220 meV) of the photoelectron spectrum taken in first order (red circles) is displayed.

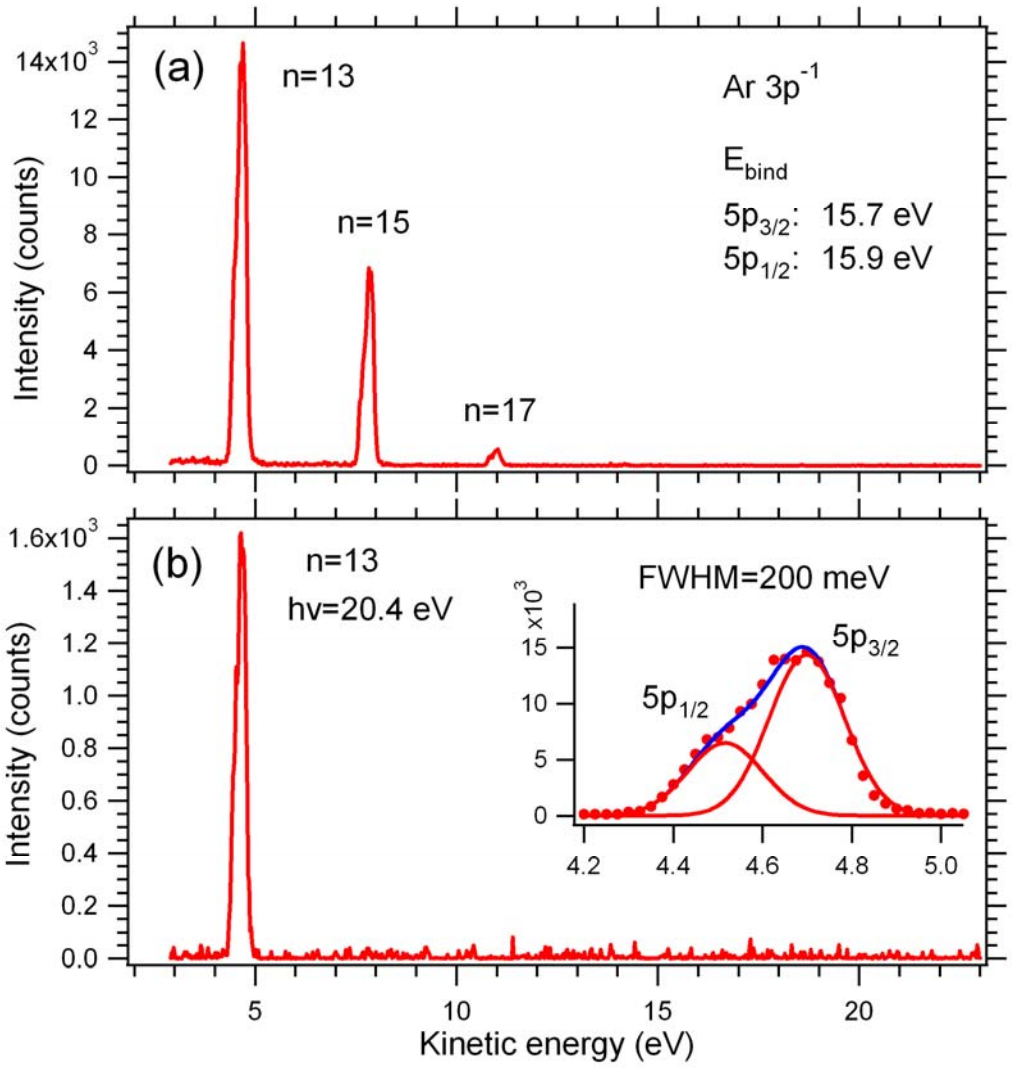

Figure 4: 3p photoelectron spectra of Ar as a sample gas taken in set up I with Xe as a generation gas and with the monochromator in zero order in (a) and in first order (selecting the 13th harmonic at 20.4 eV) in (b). In the inset in (b) a fit (blue line with two Gaussian profiles, red lines, with FWHM of 200 meV) of the photoelectron spectrum taken in first order (red circles) is displayed.

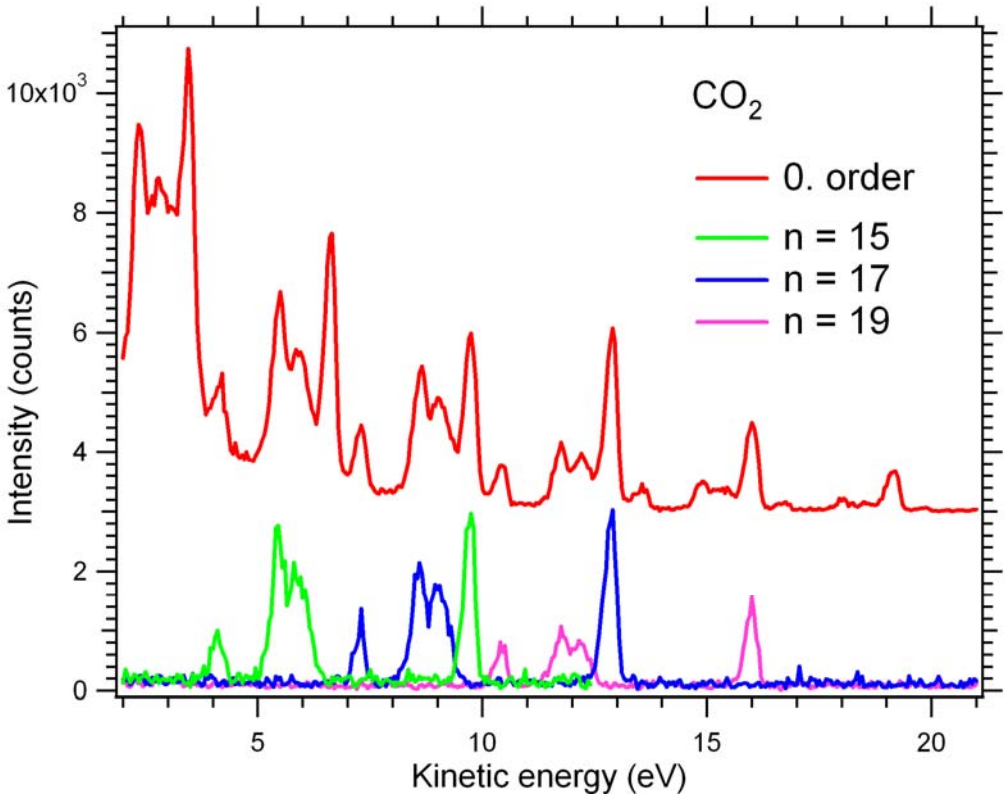

Figure 5: Photoelectron spectra of gaseous CO2 in zero order of the monochromator (red) and taken with the 15th (green, 23.6 eV), 17th (blue, 26.7 eV) and 19th harmonic (magenta, 29.8 eV). The binding energy of the main CO2 peak is 13.8 eV (96).

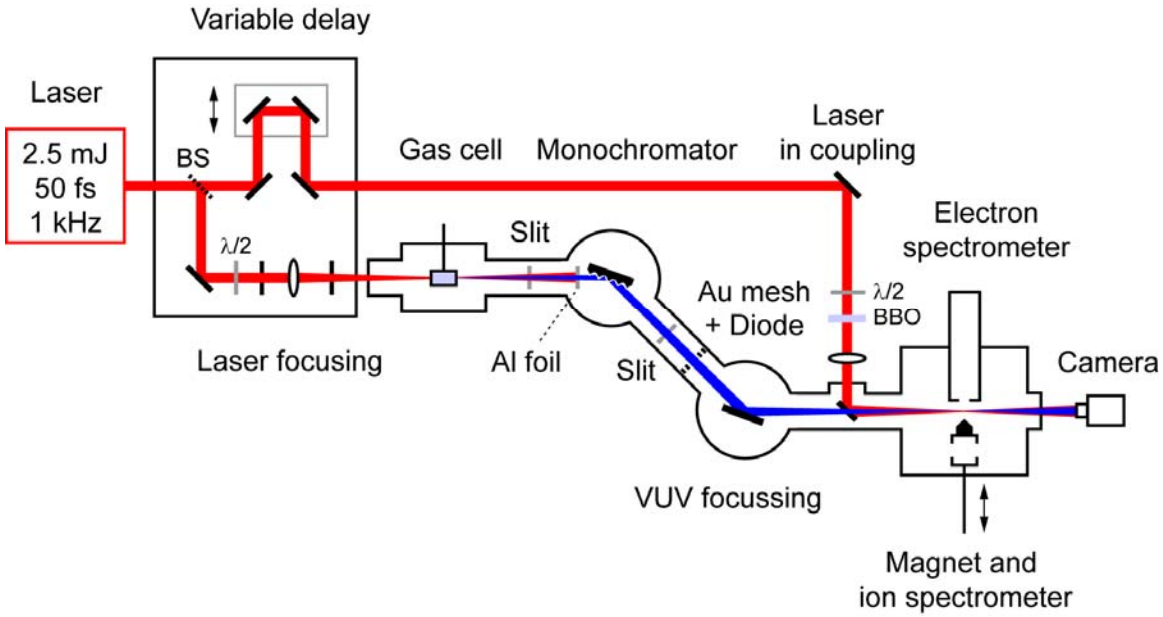

Figure 6: Schematic representation of the experimental set up (set up II) with generation of the high-order harmonics in a gas cell, with VUV focusing and with time of flight electron and ion spectrometers. BS denotes the beamsplitter and λ/2 the lambda half plates in the pump and probe parts of the laser beam.

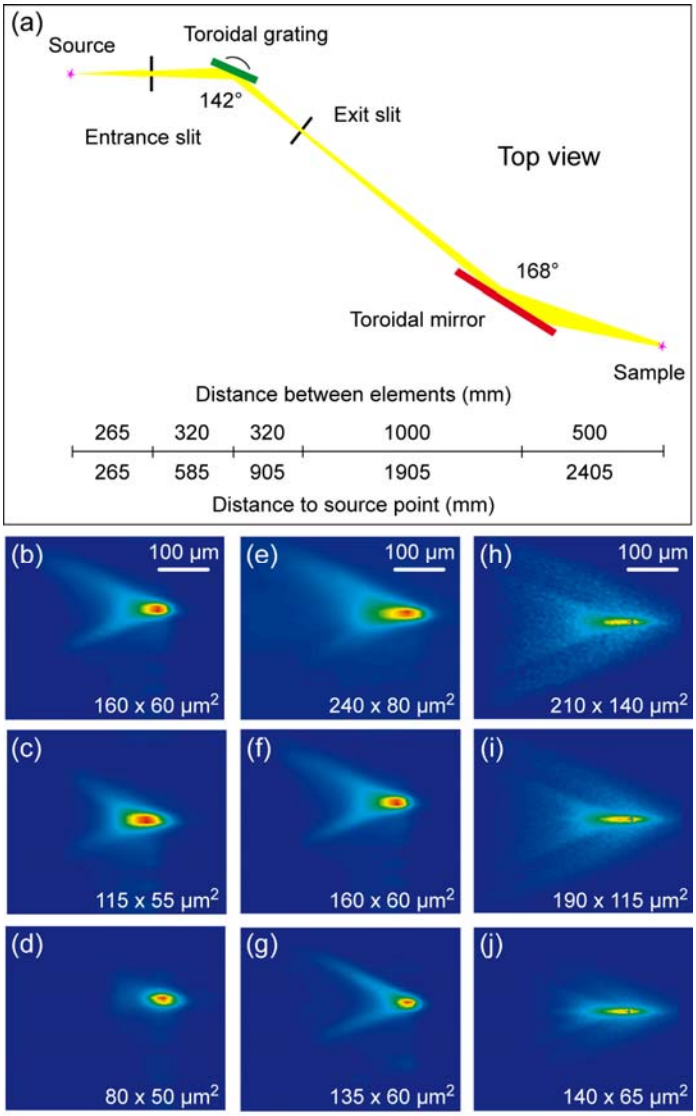

Figure 7: Measurements and simulations of the focal spot of the VUV beam in the interaction region. (a) Schematic drawing of the optical layout of set up II with relative distances between optical elements and their distances to the source in mm (drawn to scale). (b)-(g) Measured and (h)-(j) simulated focal spots (ray-tracing simulation). All given spot sizes correspond to the full width at half maximum (FWHM) in "horizontal x vertical" direction. The length of the bar in each top panel corresponds to 100 µm. (b)-(d) Measured focal spots at arbitrary generation conditions for various illuminations of the focusing mirror: (b) without baffling the beam with a focal spot size of 160x60 microns^2, (c) cutting 25% of the intensity with 115x60 microns^2 and (d) cutting 50% of the intensity with 80x50 microns^2. (e)-(g) Measured focal spots at arbitrary generation conditions for different lens positions with respect to the generation cell: (e) -10 mm, (f) +10 mm and (g) 0 mm. (h)-(j) Simulated focal spots for a beam divergence of (h) 8 mrad FWHM (full angle) and corresponding spot size of 210x140 µm^2 (i) 4 mrad and 180x116 µm^2 and (j) 2 mrad and 140x65 µm^2.

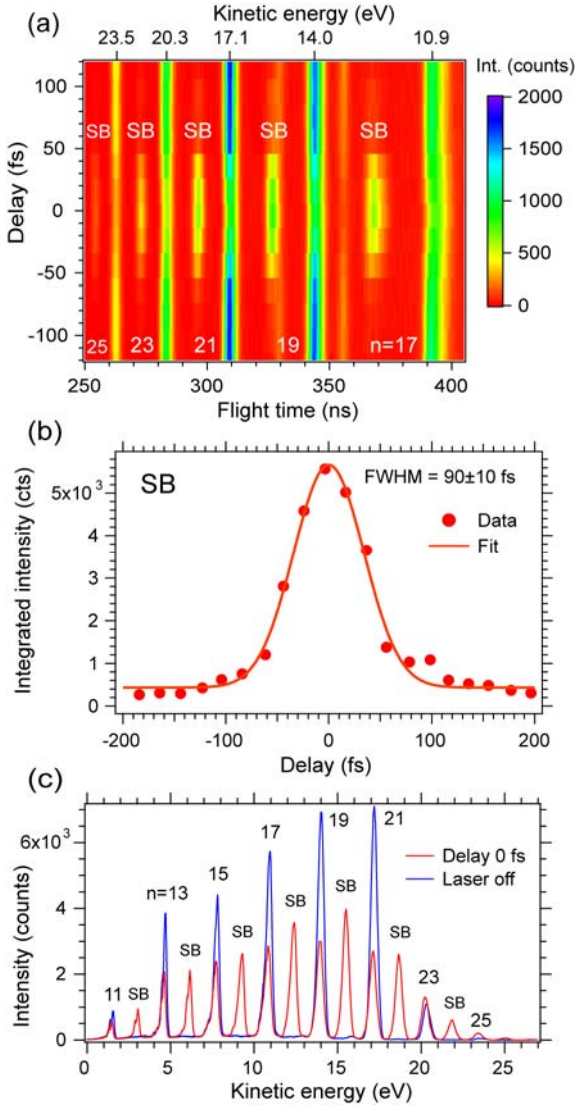

Figure 8: Ar 3p photoelectron spectra taken with Ar as a generation gas in zero order of the monochromator and with various delays between the 790 nm pump and the VUV probe pulses. (a) Spectra with main lines (n denotes the harmonic order) and side bands (SBs) versus electron flight time/kinetic energy and delay time with color coded electron counts according to the scale. (b) Integrated intensities versus delay time for the side band at a flight time of 328 ns (kinetic energy 15.6 eV, circles) with a Gaussian fit (line, FWHM 90 fs). (c) Typical Ar 3p photoelectron spectra at zero delay time (red, with main lines and the indicated harmonic orders and SBs) and without pump laser (blue, with only MLs). The spin-orbit splitting of the Ar 3p lines is not resolved.

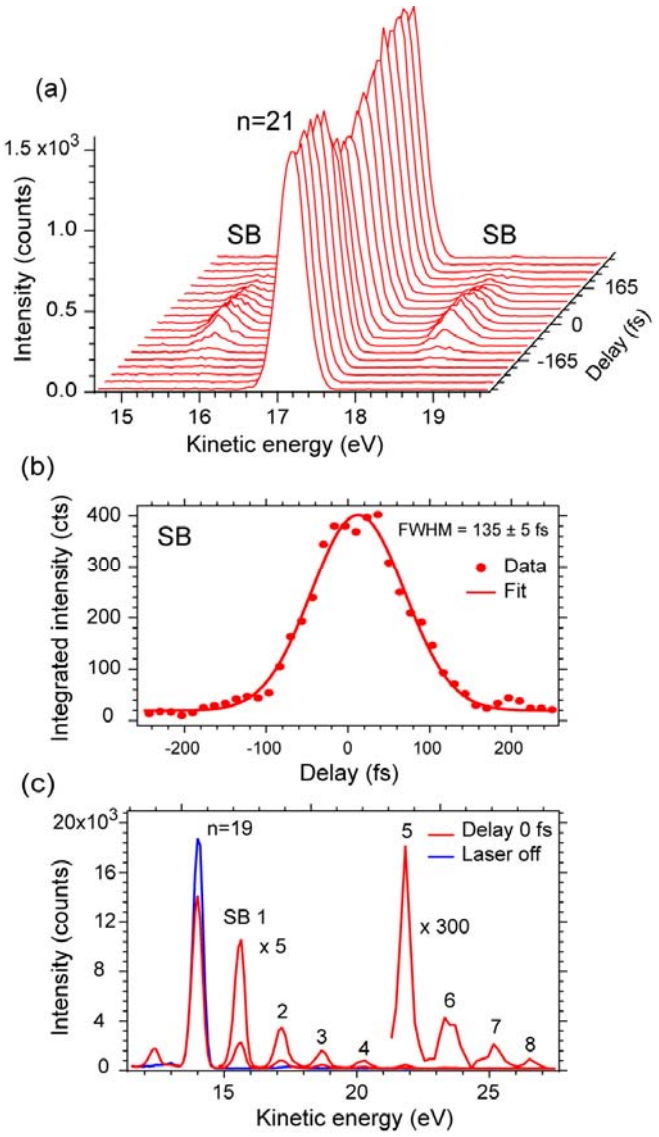

Figure 9: Ar 3p photoelectron spectra taken with Ar as a generation gas in first order of the monochromator and with various delays between the 790 nm pump and the VUV probe pulses. The spin-orbit splitting of the Ar 3p lines is not resolved. (a) Spectra taken with harmonic n = 21 (33 eV) with main lines and side bands (SBs) versus kinetic energy and delay time. (b) Cross-correlation from integrated SB intensities at 18.6 eV versus delay (circles) with a Gaussian fit (line, FWHM 135 fs). (c) Spectra taken with harmonic n = 19 (29.8 eV) at zero delay time (red, with the main line and 8 SBs, the SB on the low-energy side of the main line is not labeled) and without pump laser (blue, with only the main line). Parts of the spectrum at 0 fs delay time are multiplied by 5 and 300.

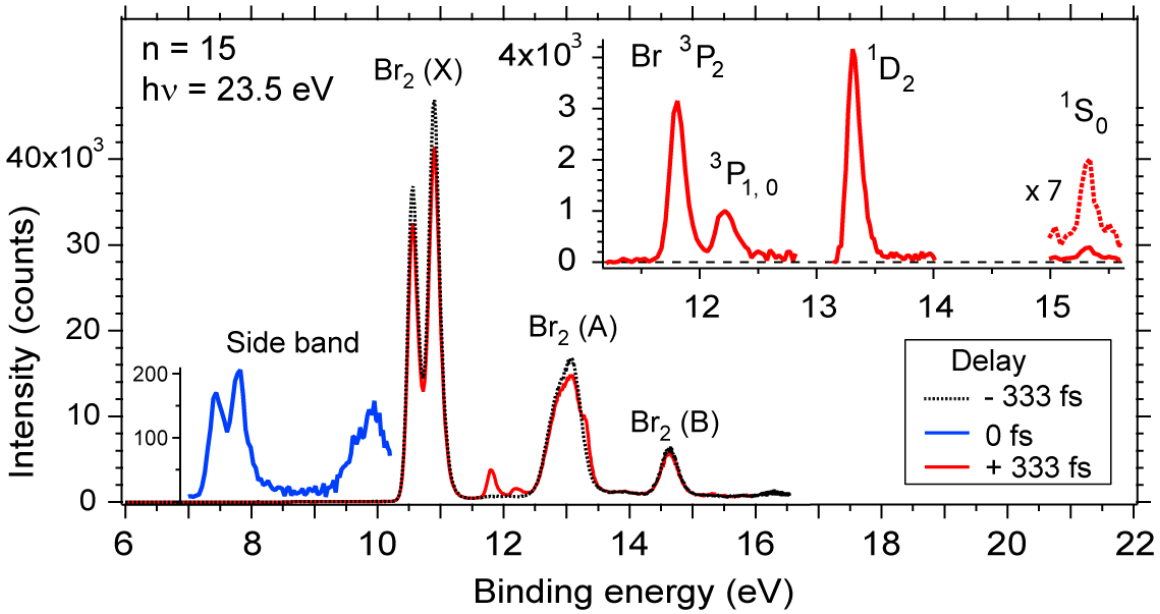

Figure 10: Photoelectron spectra of gas-phase Br_2 molecules versus binding energy at -333 fs, 0 fs and +333 fs delay between the 395 nm pump and the VUV probe pulses. Spectra were taken with the 15th harmonic (23.6 eV) with a retardation voltage of 7 V. The -333 fs spectrum serves as a reference spectrum for ground-state Br_2 molecules including all effects not depending on laser-induced dynamics. For 0 fs only the region where side-band intensities appear (7-10 eV) is shown. Atomic lines arising from photoionization of Br atoms at +333 fs are displayed separately as a difference spectrum in the inset. For this, the reference photoelectron spectrum at -333 fs was subtracted from the +333 fs spectrum. The evolution of the spectrum in the region of the ^{3}P atomic multiplet with time is shown in Fig. 11 (see ref. 45).

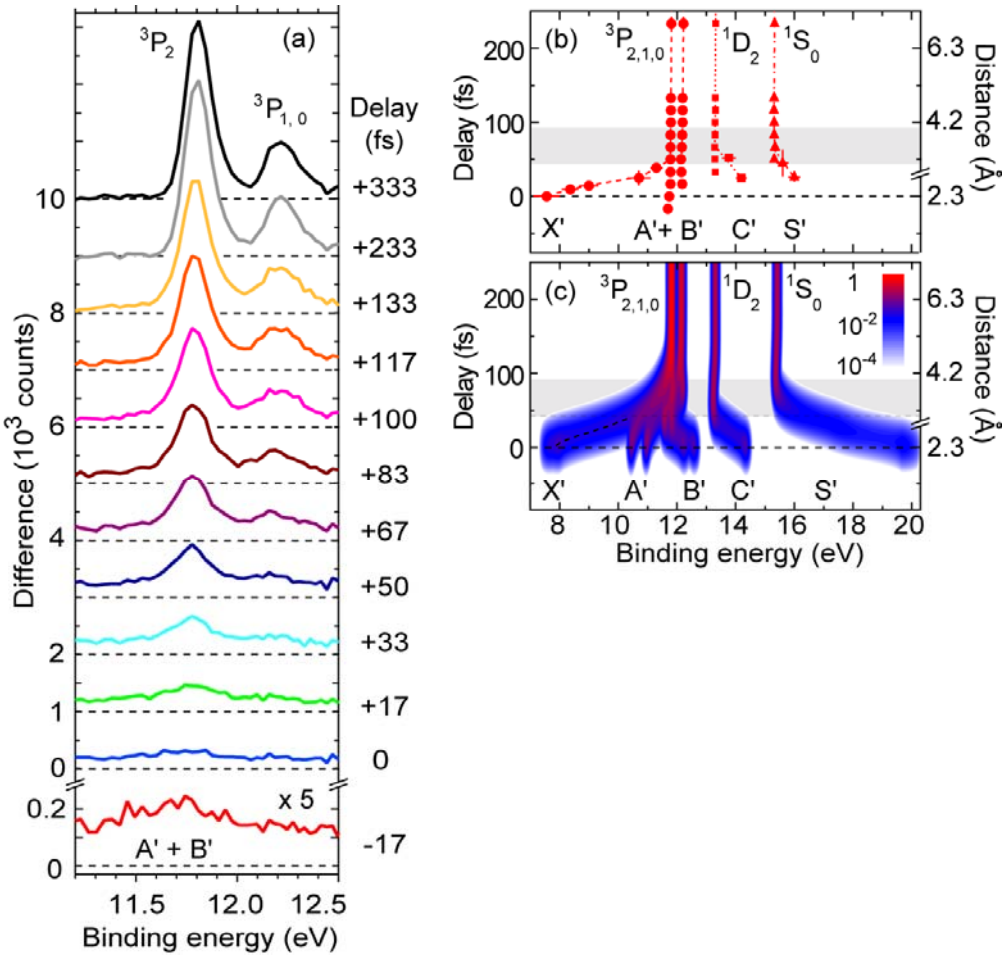

Figure 11: (a) Evolution of the photoelectron spectrum of photoexcited Br_2 in the region of the atomic ^3P multiplet from the spectrum of the excited molecule with states A' and B' at early delays to the spectrum of the free atom with the $^3P_2$, $^3P_{1,0}$ multiplet lines. The spectrum of the excited molecule at a delay of -17 fs was multiplied by 5. All spectra are difference spectra where the reference spectrum (see Fig. 10) was subtracted from the spectra at the respective delays (see ref. 100). (b) Measured binding energies of all valence states from photoexcited Br_2 molecules (X'-S') to the free atoms (^3P, ^1D, ^1S). Data points belonging to the same state are connected by lines. (c) Calculated binding energies and photoelectron intensities (color-coded logarithmic intensity scale as indicated) for Fourier-transform limited pulses of 20 fs duration and with a bandwidth of 0.1 eV. For details see ref. 45.